Organometallic Complexes for Nonlinear Optics. 66. Synthesis and Quadratic Nonlinear Optical Studies of *trans*-[Ru{C≡C{2,5-C_4H_2S-(*E*)-CH=CH}$_n$-2,5-$C_4H_2S(NO_2)$}Cl(dppe)$_2$] (n = 0-2) §

Siya Qiu,[a] Mahbod Morshedi,[b] Mahesh S. Kodikara,[c] Jun Du,[b] Yovan de Coene,[d] Chi Zhang,[a] Koen Clays,[d] and Mark G. Humphrey*,[a,b]

[a] School of Chemical Science and Engineering, Tongji University, Shanghai 200092, P. R. China

[b] Research School of Chemistry, Australian National University, Canberra, ACT 2601, Australia.

[c] Department of Chemistry, University of Ruhuna, Matara 81000, Sri Lanka.

[d] Centre for Research on Molecular Electronics and Photonics, Laboratory of Chemical and Biological Dynamics, Katholieke Universiteit Leuven, Celestijnenlaan 200D, B-3001 Leuven, Belgium.

ABSTRACT

Oligo(2,5-thienylenevinylene)s (OTVs) end-functionalized with a ligated ruthenium alkynyl unit as a donor and a nitro as acceptor, namely *trans*-[Ru{C≡C-2,5-$C_4H_2S(NO_2)$}Cl(dppe)$_2$] (**Ru1T**), *trans*-[Ru{C≡C-2,5-C_4H_2S-(*E*)-CH=CH-2,5-$C_4H_2S(NO_2)$}Cl(dppe)$_2$] (**Ru2T**), and *trans*-[Ru{C≡C-2,5-C_4H_2S-(*E*)-CH=CH-2,5-C_4H_2S-(*E*)-CH=CH-2,5-$C_4H_2S(NO_2)$}Cl(dppe)$_2$] (**Ru3T**), have been synthesized, their electrochemical properties have been assessed by cyclic voltammetry (CV), their linear optical and quadratic nonlinear optical (NLO) properties have been assayed by UV-vis-NIR spectroscopy and hyper-Rayleigh scattering studies at 1300 nm, respectively, and their linear optical properties in the formally Ru^{III} state have been examined by UV-vis-NIR spectroelectrochemistry. The data for **Ru1T**-**Ru3T** have been compared to those of the oligo(*p*-phenylenevinylene) (OPV) analogues *trans*-[Ru(C≡C-1,4-$C_6H_4NO_2$)Cl(dppe)$_2$] (**Ru1P**), *trans*-[Ru{C≡C-1,4-C_6H_4-(*E*)-CH=CH-1,4-$C_6H_4NO_2$}Cl(dppe)$_2$] (**Ru2P**), and *trans*-[Ru{C≡C-1,4-C_6H_4-(*E*)-CH=CH-1,4-C_6H_4-(*E*)-CH=CH-1,4-$C_6H_4NO_2$}Cl(dppe)$_2$] (**Ru3P**). The $Ru^{II/III}$ oxidation potentials decrease on proceeding from **Ru1T** to **Ru3T**, while the wavelength of the UV-vis λ_{max} band increases on proceeding from **Ru1T** to **Ru2T**, but thereafter decreases on further progression to **Ru3T**, similar trends to those seen proceeding from **Ru1P** to **Ru3P**. The quadratic nonlinearity β_{1300} increases on OTV lengthening from **Ru1T** through **Ru2T** to **Ru3T**; the data are significantly larger than those of the **Ru1P**-**Ru3P** analogues which peak at **Ru2P**. The formally Ru^{III} complexes exhibit low-energy bands that red-shift significantly on proceeding from **Ru1T** to **Ru3T**. Computational studies employing time-dependent density functional theory were undertaken on model

complexes to rationalize the optical observations and explore the impact of further OTV bridge lengthening. Computational studies on model complexes **Ru1T'-Ru6T'** are consistent with decreasing contributions of the electron donor (ligated Ru) and acceptor (NO_2) groups to the HOMO and LUMO, respectively, upon π-bridge lengthening. β_{tot} values increase on progression from **Ru1T'** to **Ru3T'**, but thereafter further bridge lengthening affords little further increase in β_{tot}, consistent with a saturation in quadratic NLO response.

Keywords: Alkynyl complexes; Molecular electrochemistry; Nonlinear optics; Transition metals

---

* Corresponding author: *E-mail*: Mark.Humphrey@anu.edu.au.

§ Dedicated to Dr Jean-René Hamon on the occasion of his 65th birthday.

1. Introduction

Conducting polymers are of potential or demonstrated importance for a broad range of uses in organic light-emitting diodes, supercapacitors, sensors, solar cells, printed circuits, and displays. π-Delocalizable poly(*p*-phenylenevinylene) (PPV) and poly(2,5-thiophene) (PT) are prime examples of polymers that have been studied for such applications. Poly(2,5-thienylenevinylene) (PTV) is related to both PPV and PT in that it corresponds to replacement of the 1,4-phenylene groups in PPV with 2,5-thienylene units, and also corresponds to insertion of (*E*)-ene linkages between the 2,5-thienylene repeating units of PT, but PTV has been less studied than PPV or PT. It is axiomatic that the improvement of polymeric materials is facilitated by the development of structure-property relationships for corresponding well-defined systematically-varied oligomers; studies of specific oligo(2,5-thienylenevinylene)s (OTVs) are therefore of significant interest because the well-defined optical properties of monodisperse OTV species can model aspects and advance understanding of PTV. Functionalization of OTVs with organic solubilizing groups has been pursued to enhance understanding of PTV [1,2], but the end-functionalization of OTVs with ligated metal units has been much less explored [3], despite the potential advantages that this may endow (as well as enhanced solubility, the metal unit in the resultant metallopolymer may imbue the oligomer/polymer with redox behavior, novel optical and/or magnetic properties, etc.) [4,5]. Notwithstanding the dearth of prior studies, metal-appended OTVs are therefore of significant interest.

In addition to linear optical properties such as absorption and (electro)luminescence that are of importance for some of the applications above, the nonlinear optical (NLO) properties of molecular materials have also come under considerable scrutiny. Significant NLO properties are found in molecules with readily polarizable charge distributions. Organic molecules and polymers with π-delocalizable components have been shown to possess appreciable optical nonlinearities and ultrafast responses. Organometallic complexes have also attracted attention; they have the benefits of organic compounds, but in addition have considerably greater compositional variability. Early studies involved examination of a plethora of organometallic complex types, but attention has focussed on metallocenyl and alkynyl complexes [6,7]. Alkynyl complexes, in particular, have been of significant recent interest because certain examples have afforded record NLO coefficients [8-12].

As summarized above, organometallic OTVs are intriguing species and metal alkynyl complexes have demonstrated strong NLO efficiency, but surprisingly there have been few studies of the NLO properties of OTVs end-functionalized by metal alkynyl units [13-16], and none exploring the OTV bridge-length-dependence of electrochemical, linear optical, and NLO properties. We report herein the syntheses of a systematically bridge-lengthened series of ruthenium complexes with OTV-alkynyl ligands end-functionalized with nitro groups, together with studies exploring the electrochemical, linear optical and quadratic nonlinear optical properties of these donor-bridge-acceptor (D-B-A) dipolar compounds,

comparisons to previously reported oligo(phenylenevinylene) bridge-containing analogues, and theoretical studies rationalizing the experimental observations.

2. Results and discussion

2.1. Syntheses and Characterization. A considerable body of prior work has identified dipolar compounds with a D-B-A composition as efficient quadratic NLO-active materials [17], so complexes with this composition were selected as targets in the present studies. The assembly of OTVs end-functionalized with ligated Ru and nitro groups necessitated the construction of organic OTVs end-functionalized by terminal alkyne and nitro groups, which could then be reacted with the metal precursor. The *trans*-[RuCl(dppe)$_2$] unit (dppe = 1,2-bis(diphenylphosphino)ethane) can function as a strong donor and, as a result, it has been employed in the construction of alkynyl complexes with significant NLO properties and additional useful functionality (reversible redox behavior, intense optical transitions) [18,19]. [RuCl(dppe)$_2$]-containing alkynyl complexes can be obtained in a straightforward fashion from reaction of [RuCl(dppe)$_2$]$^+$ with the terminal alkyne in the presence of a large non-coordinating counter-ion, followed by treatment with base [20-22].

In contrast to the smaller alkynes 5-ethynyl-2-nitrothiophene and 1-(2-nitrothien-5-yl)-2-(5-ethynylthien-2-yl)-(*E*)-ethene, the next-longer homologue was unknown and consequently was synthesized for these studies (Scheme 1). 5-(Bromomethyl)-2-nitrothiophene was reacted with triethylphosphite to give the corresponding phosphonate ester diethyl {(5-nitrothiophen-2-yl)methyl}phosphonate (**1**) in excellent yield. The phosphonate ester was reacted with 1-(2-bromothien-5-yl)-2-(2-formylthien-5-yl)-(*E*)-ethene under Wadsworth-Emmons-Horner conditions to afford 2-bromo-5-{(*E*)-2-(5-{(*E*)-2-(5-nitrothiophen-2-yl)ethenyl}thiophen-2-yl)ethenyl}thiophene (**2**) in good yield. Sonogashira coupling of **2** with ethynyltrimethylsilane and subsequent desilylation with carbonate gave 2-ethynyl-5-{(*E*)-2-(5-{(*E*)-2-(5-nitrothiophen-2-yl)ethenyl}thiophen-2-yl)ethenyl}thiophene (**4**) in very good yield. The alkynes were then reacted with [RuCl(dppe)$_2$]PF$_6$, followed by treatment with base, to give the new complexes **Ru1T**, **Ru2T**, and **Ru3T** (Scheme 1). Detailed information on synthetic procedures are given in the Experimental section.

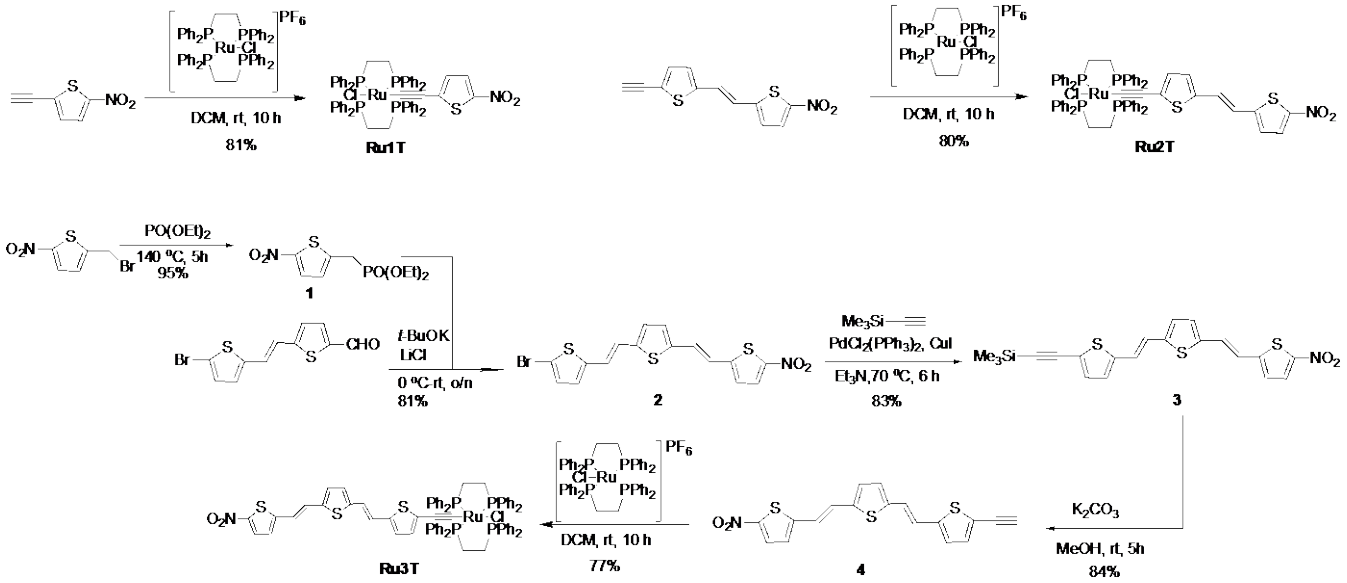

Scheme 1. Syntheses of **1-4** and **Ru1T**-**Ru3T**.

All compounds were characterized by the usual spectroscopic and spectrometric techniques (Figures S1-S18), and the molecular structures of **Ru1T** and **Ru2T** were confirmed by single-crystal X-ray crystallographic studies (Figures 1, 2, S19, and S20, and Table S1). The ^{31}P NMR spectra of the complexes **Ru1T**, **Ru2T**, and **Ru3T** exhibit singlets at 48.0, 48.8, and 48.9 ppm, respectively, consistent with *trans* stereochemistry at a mono-alkynyl bis(dppe)ruthenium centre, while the IR spectra contain characteristic ν(C≡C) bands that move to higher energy on bridge lengthening (**Ru1T**: 2022, **Ru2T**: 2034, **Ru3T**: 2038 cm^{-1}), consistent with an increasingly remote nitro acceptor group becoming increasingly ineffective at removing electron density from the thienyl ring proximal to the metal, and thereby disfavouring the Ru^{+}=C=C=thienyl^{-}-containing resonance contributor that reduces C_{Ru}-$C_{thienyl}$ bond order. The identities of all three complexes were confirmed by their ESI mass spectra which contain commonly observed ions corresponding to loss of chloro from the molecular ion [23,24]. The bond lengths and angles from the structural study of **Ru2T.2CH$_2$Cl$_2$** are unremarkable. The structural study of **Ru1T** revealed positional disorder of the chloro and alkynyl ligands, the model for which resulted in a somewhat short Ru1-Cl1 distance, an unusually long Ru-C1 vector, and a cigar-shaped C1 thermal ellipsoid; as such, it is inappropriate to comment on bond lengths at the chloro-Ru-alkynyl region, but the structural study of **Ru1T** does confirm the atomic connectivity.

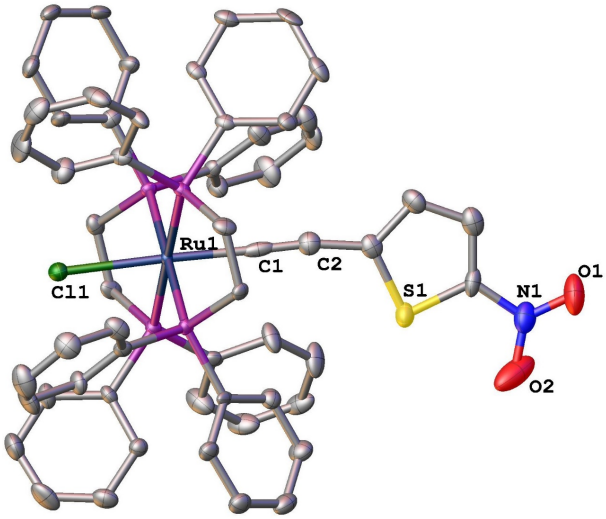

Figure 1. Molecular structure of **Ru1T**, with thermal ellipsoids set at the 40% probability level. Hydrogen atoms have been omitted for clarity. Selected bond lengths (Å) and angles (°): Ru1-P1 2.3434(16), Ru1-P2 2.3766(17), Ru1-P3 2.3574(16), Ru1-P4 2.3858(16), Ru1-Cl1 2.472(2), Ru1-C1 2.057(11), C1-C2 1.153(13), P1-Ru1-P2 81.67(6), P1-Ru1-P3 179.52(8), P1-Ru1-P4 98.04(6), P2-Ru1-P3 98.80(6), P2-Ru1-P4 179.62(8), P3-Ru1-P4 81.50(6), P1-Ru1-Cl1 93.39(6), P2-Ru1-Cl1 100.37(6), P3-Ru1-Cl1 86.64(6), P4-Ru1-Cl1 79.88(6), P1-Ru1-C1 87.5(3), P2-Ru1-PC1 82.9(3), P3-Ru1-C1 92.4(3), P4-Ru1-C1 96.9(3), Cl1-Ru1-C1 176.7(3).

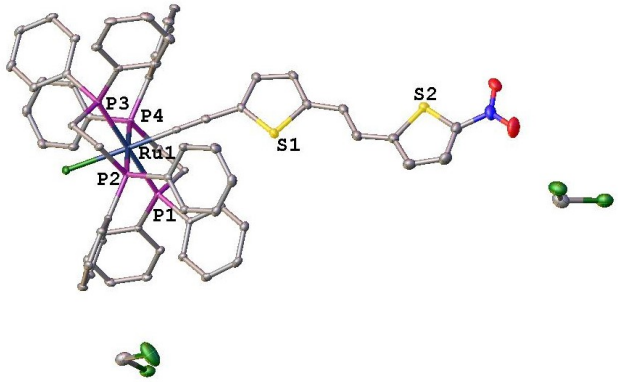

Figure 2. Molecular structure of **Ru2T.2CH$_2$Cl$_2$**, with thermal ellipsoids set at the 40% probability level. Hydrogen atoms have been omitted for clarity. Selected bond lengths (Å) and angle (°): Ru1-P1 2.3815(6), Ru1-P2 2.3726(6), Ru1-P3 2.3797(6), Ru1-P4 2.3556(6), Ru1-Cl1 2.5058(6), Ru1-C1 1.994(3), C1-C2 1.196(4), P1-Ru1-P2 97.79(2), P1-Ru1-P3 179.66(2), P1-Ru1-P4 82.27(2), P2-Ru1-P3 82.06(2), P2-Ru1-P4 178.36(2), P3-Ru1-P4 97.87(2), P1-Ru1-Cl1 98.04(2), P2-Ru1-Cl1 88.44(2), P3-Ru1-Cl1 82.26(2), P4-Ru1-Cl1 93.18(2), P1-Ru1-C1 82.88(7), P2-Ru1-C1 91.86(7), P3-Ru1-C1 96.82(7), P4-Ru1-C1 86.52(7) , Cl1-Ru1-C1 178.99(7).

2.2 Linear optical properties. UV-vis absorption maxima and extinction coefficients for **Ru1T**-**Ru3T**, together with data for the oligo(phenylenevinylene)-containing analogues *trans*-[Ru(C≡C-1,4-$C_6H_4NO_2$)Cl(dppe)$_2$] (**Ru1P**), *trans*-[Ru{C≡C-1,4-C_6H_4-(*E*)-CH=CH-1,4-$C_6H_4NO_2$}Cl(dppe)$_2$] (**Ru2P**), and *trans*-[Ru{C≡C-1,4-C_6H_4-(*E*)-CH=CH-1,4-C_6H_4-(*E*)-CH=CH-1,4-$C_6H_4NO_2$}Cl(dppe)$_2$] (**Ru3P**), are collected in Table 1 (the spectra are provided in Figures S21-S23). The low-energy optical absorption maximum red-shifts on proceeding from **Ru1T** to **Ru2T** and then blue-shifts on proceeding from **Ru2T** to **Ru3T**; a similar behaviour is seen on proceeding from **Ru1P** to **Ru2P** and then **Ru3P**. For the latter, the low-energy band has been assigned to a LUMO ← HOMO MLCT transition with significant ruthenium involvement in the HOMO and nitro contribution to the LUMO, and with decreasing contribution of the Ru and NO_2 and an increasingly OPV-centred transition on OPV lengthening [25,27,28]. The computational studies on the present series of complexes are summarized below.

Table 1. Cyclic voltammetric and linear optical data.

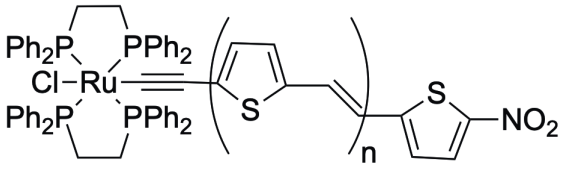

n = 0 (**Ru1T**), 1 (**Ru2T**), 2 (**Ru3T**)

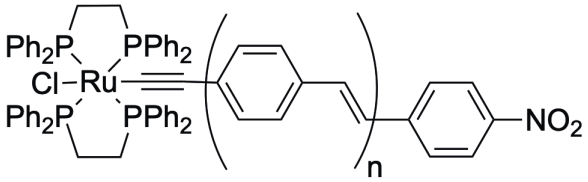

n = 0 (**Ru1P**), 1 (**Ru2P**), 2 (**Ru3P**)

	Ru oxidation[a)]	NO_2 reduction[a)]	ν_{max} [ε] Ru^{II} [b)]	ν_{max} [ε] Ru^{III} [b)]	Ref
Ru1T	0.78 [134, 1]	-1.11 [124, 1]	18,500 [2.6]	11,050 [0.6]	This work
Ru2T	0.52 [78, 1]	-0.81 [94, 1]	16,550 [2.7]	9,050 [1.1]	This work
Ru3T	0.46 [66, 1]	-0.71 [55, 1]	17,050 [3.2]	7,800 [1.9]	This work
Ru1P	0.74 [c, 0.9]	-0.84 [c, 0.8]	20,950 [2.0][d)]	c)	[25]
Ru2P	0.55 [c, 1]	-0.98 [c, 1]	20,450 [2.6][d)]	c)	[25]
Ru3P	0.54 [c, 1]	-0.91 [c, 0.9]	21,350 [1.6][d)]	c)	[26]

Measured in CH_2Cl_2; a) $E_{1/2}$ (V) [ΔE (V), i_{pc}/i_{pa}], FcH/FcH^+ couple at 0.56 V ($\Delta E \approx 0.2$ V, $i_{pc}/i_{pa} \approx 1$), Fc = ferrocenyl; b) cm^{-1} [10^4 M^{-1} cm^{-1}]; c) not reported; d) measured in THF.

2.3 Electrochemical and spectroelectrochemical studies. The results from cyclic voltammetric studies on **Ru1T**, **Ru2T** and **Ru3T** (Figures S24-S26) reveal a fully reversible oxidation process for each complex that occurs at decreasingly positive potentials on proceeding from **Ru1T** to **Ru3T** (ΔRu_{ox} 0.32 V), a similar but more accentuated trend to that seen on proceeding from **Ru1P** to **Ru3P** (ΔRu_{ox} 0.20 V), and analogous to that seen with dipolar ruthenium alkynyl complexes with OPE π-bridges [29]; as the π-bridges increase in length, the electron-withdrawing influence of the nitro groups is attenuated, rendering the complexes easier to oxidize. The HOMO becomes increasingly bridge-centred on lengthening the bridge, rendering the more electron-rich thienyl-based bridges in **Ru1T**-**Ru3T** increasingly easier to oxidize than **Ru1P**-**Ru3P** for comparable bridge length upon bridge lengthening. In contrast to the **Ru1P**-**Ru3P** series, the bridge lengthening on proceeding from **Ru1T** to **Ru3T** renders the complex increasingly easier to reduce (Table 1).

In situ UV-vis spectroelectrochemical studies using an OTTLE (optically transparent thin-layer electrochemical) cell allows simultaneous collection of spectra whilst the complex is undergoing a redox process. New low-energy bands (with clean isosbestic points) appear after application of a 0.8-0.9 V potential to a sample of each complex (Figures 3, S27 and S28); these new bands shift to lower energy and increase in number and intensity on π-bridge lengthening. These oxidation processes are fully-reversible and are clearly accompanied by strong optical changes. We have previously demonstrated that such complexes are candidates for nonlinear optical switching [30-33], but we have not pursued this possibility in the present studies.

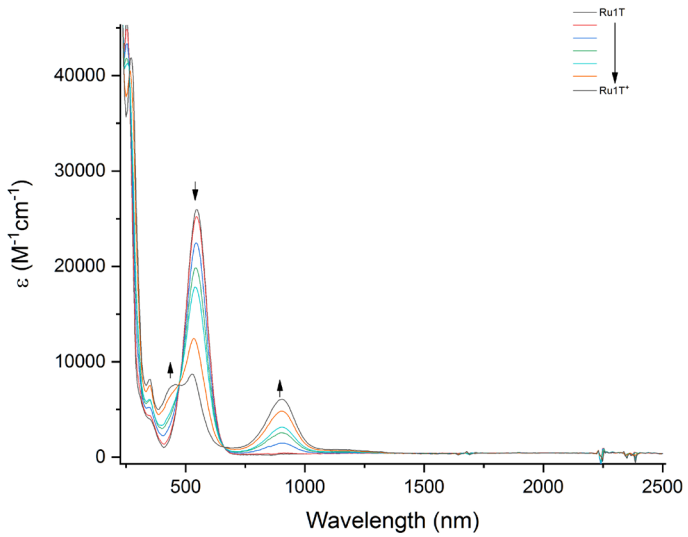

Figure 3. Progressive changes to the UV-vis-NIR spectrum for complex **Ru1T** on application of a 0.9 V potential.

2.4 Hyper-Rayleigh scattering studies. The quadratic nonlinearities of **Ru1T**-**Ru3T** were determined at 1300 nm using the hyper-Rayleigh scattering technique, and correcting (where required) for multi-photon fluorescence and self-absorption; the results are presented in Table 2, together with the two-level corrected values and the corresponding data for **Ru2P**-**Ru3P** [26]. Two-level corrections to afford frequency-independent nonlinearities have been employed widely, and the shortcomings have been critiqued (see, for example, ref. 25). The model was developed for 1D molecules with a dominant charge-transfer transition, which is rarely the case for organometallics, but if applied cautiously it may be useful where structural variations are restricted to the components responsible for the low-energy charge-transfer, as in the present study: for **Ru1T**-**Ru3T**, the low-energy bands involve the alkynyl ligand that is the subject of systematic variation. We have therefore also explored the evolution of two-level model-generated β_0 upon structural modification (while being cognizant of the aforementioned shortcomings).

Table 2. Summary of HRS results.

Complex	$\lambda_{max,}$ (nm)[a)]	$<\beta>_{HRS}$[b)]	$<\beta_0>$[c)]	Ref.
Ru1P	477	n.m.	n.m.	26
Ru2P	489	60 ± 2[d)]	22 ± 1	26
Ru3P	468	33 ± 2[d)]	14 ± 1	26
Ru1T	541	210 ± 12	53 ± 3	This work
Ru2T	604	1300 ± 80	140 ± 9	This work
Ru3T	586	1500 ± 210	230 ± 30	This work

a) Solvent THF. b) Measured in THF at 1300 nm; HRS values in units of 10^{-30} esu. c) Corrected for resonance enhancement at 650 nm using the two-level model with $\beta_0 = \beta[1-(2\lambda_{max}/1300)^2][1-(\lambda_{max}/1300)^2]$. d) Converted from the β_{zzz} values in ref. 26. n.m. = not measurable.

The present study is focused on assessing the influence of OTV π-bridge lengthening. On moving from **Ru1T** to **Ru2T**, $<\beta>_{HRS}$ and $<\beta_0>$ undergo significant increases, but a smaller increase is observed on further lengthening to afford **Ru3T**. The smaller increase on subsequent lengthening is consistent with an approach to saturation; similar trends have been seen with OPE- and OPV-bridged analogues [26,28,29]. An additional important concern is to assess the relative merit of π-bridge construction via OTV groups, and in particular to contrast this performance to similar length complexes with bridges consisting of OPV or OPE units. We have previously shown that OPV bridges are superior to OPE bridges of comparable length. Comparison of the data in Table 2 for equivalent length π-bridges shows that OTV-bridged

complexes are superior to the OPV-bridged analogues. The molecular first hyperpolarizabilities of the OTV complexes are large, but the charge-transfer absorption band maxima are close to the second-harmonic wavelength (650 nm); this, coupled to the aforementioned problems with the two-level approximation, render further comments unjustifiable. Studies at longer wavelengths remote from the optical absorption bands are needed for a more detailed analysis.

2.5 Computational studies. Computational studies employing density functional theory (DFT) and time-dependent DFT (TD-DFT) were undertaken to rationalize the optical properties of the complexes in the present study and to suggest the behavior of examples with longer OTV bridges. In the case of **Ru1T**, **Ru2T**, and **Ru3T**, hydrogens were used in place of the phenyl groups of the diphosphine ligands, the resultant theoretical species being hereafter denoted as **Ru1T'**, **Ru2T'**, and **Ru3T'**, while DFT/TD-DFT studies were also undertaken on **Ru4T'**, **Ru5T'**, and **Ru6T'** (for complexes with four, five, and six thienyl groups, respectively). Details of the calculations are given in the Supplementary data. Table 3 summarizes the DFT/TD-DFT data for **Ru*n*T'** (***n*** = 1-6).

Table 3. Summary of DFT and TD-DFT calculations.

Model[a)]	β_{tot}[b)] (10^{-30} esu)	Wavenumber (cm^{-1})]	Oscillator strength	Composition (weight %)
Ru1T'	164.33 (1.0)	25063	0.753	HOMO → LUMO (96)
Ru2T'	723.77 (4.4)	20450	1.473	HOMO → LUMO (87)
Ru3T'	1247.53 (7.6)	18797	2.119	HOMO → LUMO (74)
Ru4T'	1547.73 (9.4)	18018	2.830	HOMO → LUMO (57)
Ru5T'	1672.51 (10.2)	17575	3.545	HOMO → LUMO (44) HOMO → LUMO+1 (29)
Ru6T'	1724.92 (10.5)	17241	4.263	HOMO → LUMO+1 (34) HOMO → LUMO (31)

a) Experimental analogues of **Ru4T'**–**Ru6T'** were not synthesized. b) Static total first hyperpolarizability (see Supplementary data). The ratio β(Model):β(**Ru1T'**) is shown in parentheses.

The π-conjugated bridges of **Ru2T'**-**Ru6T'** consist of thienyl and ethenyl units connected by rotatable single bonds. The barrier to rotation about such bonds is low [34]. Calculated relative energies for the different rotamers of **Ru3T'** in the present study suggest that several rotamers can coexist under laboratory conditions (see Supplementary data). The lowest-energy coplanar rotamer of **Ru3T'** has the four single bonds that can rotate oriented such that a transoid (*t*) configuration is found at each bond (the transoid configurations correspond to the two double bonds joined by the thienyl-ethenyl single bond being trans disposed with respect to one another). We consequently adopted this configuration – in which every

thienylene-vinylene single bond in the conjugated backbone exists in the *t* configuration – for the initial structures of **Ru*n*T'** (***n*** = 2-6), permitting comparison of complexes with differing bridge lengths.

The static total first hyperpolarizabilities (β_{tot}), excitation energies (cm^{-1}), and oscillator strengths for the optimized model complexes, **Ru*n*T'** (***n*** = 1-6), were calculated in THF solvent (Table 3). The calculated quadratic NLO responses increase upon alkynyl ligand π-bridge lengthening. A significant increase in β_{tot} results on proceeding from **Ru1T'** to **Ru2T'**. The calculated first hyperpolarizability increases (but less profoundly) upon lengthening the bridge further, proceeding from **Ru2T'** to **Ru3T'**. These DFT predictions are consistent with the HRS and two-level corrected hyperpolarizabilities of their experimental analogues. There is no substantial difference in the calculated hyperpolarizabilities of the longer π-bridge complexes; for example, the difference between β_{tot} values of **Ru5T'** and **Ru6T'** is only ca. 50×10^{-30} esu, indicating that β saturates at longer π-bridge lengths for the model complexes.

Bridge lengthening affects the stability of the frontier orbitals of the model complexes; as a result, the calculated HOMO-LUMO gap continues to decrease with increasing bridge length (in contrast to the β_{tot} values). Table 4 presents the DFT HOMO-LUMO gaps (Δ_{H-L}) and the composition of the frontier orbitals for **Ru*n*T'** (***n*** = 1-6). There is an inverse relationship between β_{tot} and Δ_{H-L}, but increasing the bridge length beyond that of **Ru3T'** has a minor effect on Δ_{H-L}. According to Table 4, bridge lengthening leads to an increase in the energy of HOMOs and a decrease in the energy of LUMOs, resulting in a reduction in the HOMO-LUMO gap, but for longer π-bridge complexes, the effect on the orbital energies is less profound. Orbital compositions show that the HOMOs and the LUMOs are increasingly localized on the thienylenevinylene unit for complexes **Ru*n*T'** (***n*** = 3-6), with concomitant reduction in the metal and the nitro character.

Table 4. DFT HOMO-LUMO gaps (Δ_{H-L}) and percentage contributions to the HOMO (H) and LUMO (L).[a)]

Model		Energy (eV)	Δ_{H-L} (eV)	Ru	Cl	P	C_2	B	NO_2
Ru1T'	L	-1.57	5.26	1	0	1	7	40	51
	H	-6.83		31	4	2	32	27	4
Ru2T'	L	-1.95	4.33	0	0	0	2	62	36
	H	-6.28		17	1	2	24	54	2
Ru3T'	L	-2.09	3.97	0	0	0	1	70	29
	H	-6.06		11	1	1	18	68	1
Ru4T'	L	-2.14	3.82	0	0	0	0	74	26
	H	-5.96		8	1	1	14	76	0
Ru5T'	L	-2.17	3.73	0	0	0	0	76	24

	H	-5.90		6	0	1	11	82	0
Ru6T'	L	-2.18	3.69	0	0	0	0	78	22
	H	-5.87		5	0	1	10	84	0

a) C_2 = alkynyl carbons, P = phosphine co-ligands, B = thienyl (**Ru1T'**)/thienylenevinylene units (**Ru*n*T'**, ***n*** = 2-6).

Table 3 reports the calculated excitation energies and oscillator strengths of the low-energy transitions for the model complexes, together with the principle molecular orbitals involved. The linear optical properties were obtained in THF. The calculations predict a strong low-energy transition in the visible region for all model systems. A significant red-shift in the low-energy absorption band is found on proceeding from **Ru1T'** to **Ru2T'**, consistent with the observation of their experimental counterparts, although the estimated energies are blue-shifted compared to the laboratory values. On the basis of the orbital compositions in Table 4, these transitions are primarily MLCT in character. Proceeding from **Ru2T'** to **Ru3T'** causes a red-shift in the HOMO → LUMO transition. The opposite outcome was observed experimentally but, as mentioned earlier, the calculations for the model complexes were undertaken on a single conformer in which the double bonds about the thienylene-vinylene single bond are disposed in a transoid (*t)* configuration. As shown in Table S2, different conformers, which have nearly identical energies, exhibit different first hyperpolarizabilities and excitations, and for some rotamers (e.g. *tccc*), the excitation energies are actually higher than that of the *tttt* rotamer, so the conformational variability in the OTV bridge may be a reason for the abovementioned mismatch. In the case of longer π-bridge complexes, the position of the computed low-energy band hardly changes. For example, the shift towards longer wavelengths is only ca. 300 cm^{-1} on proceeding from **Ru5T'** to **Ru6T'**, and the transitions show increasing OTV-centred character upon lengthening. The calculations reveal an almost linear correlation between the calculated optical nonlinearities of the model complexes and wavelength of the low-energy transitions (Figure S30), consistent with the importance of the low-lying intense transitions for their quadratic NLO responses.

3. Conclusion

The present study has afforded the complexes **Ru1T**-**Ru3T**, which comprise a set of end-functionalized OTV-containing dipolar organometallics that are analogues of previously reported OPV-bridged examples. The resultant suite of systematically-varied OTV/OPV complexes has enabled us to explore the effect of bridge variation and lengthening on electrochemical and optical properties. Bridge lengthening leads to an increased ease in oxidation for both the OTV and OPV series, consistent with the diminishing influence of the increasingly remote nitro acceptor group. Both series of complexes exhibit

low-energy bands in their UV-vis-NIR spectra, with the band maxima for the OTV examples uniformly red-shifted compared to their OPV analogues; the underlying transitions are MLCT in nature for **Ru1T**/**Ru1P**, but become increasingly bridge-centred on progressing to **Ru2T**/**Ru2P** and then **Ru3T**/**Ru3P**. In the case of the **Ru1T**-**Ru3T** series, we have also explored their UV-vis-NIR spectroelectrochemical behaviour; oxidation affords strong low-energy LMCT bands in the NIR that red-shift upon bridge lengthening.

Quadratic optical nonlinearities increase on bridge lengthening in the OTV series, in contrast to the OPV series for which a maximum is reached at the 2PV example. Absolute values for the OTV complexes are significantly larger (more than an order of magnitude) than their OPV analogues, a performance improvement that persists in a reduced fashion upon proceeding to two-level-corrected data. The experimental data are unambiguous in identifying the OTV series as superior.

There are a couple of notable shortcomings with a purely experimental approach. The experimental complexes can undergo facile rotation about bonds in the bridges, affording a large number of conformers in solution (the combination of which are assessed with the experimental measurements). Furthermore, defining the saturation length of such systems necessitates exploring further π-bridge lengthening, but this increases the synthetic expense significantly. For both of these reasons, computational studies are beneficial. In the present work, we have explored theoretical analogues of the OTV series (including thus-far-not-synthesized higher homologues), and observed increasing β_{tot} values proceeding to **Ru6T'**, but we also noted evidence of saturation of response at the higher members of the series. The computational studies also enabled us to explore the NLO performance of individual conformers, noting significant differences in their hyperpolarizability tensors, a comparison that is not experimentally possible.

4. Experimental

4.1 Materials. The compounds 5-ethynyl-2-nitrothiophene [35], 1-(2-nitrothien-5-yl)-2-(5-ethynylthien-2-yl)-(*E*)-ethene [13], 5-bromomethyl-2-nitrothiophene [36], 1-(2-bromothien-5-yl)-2-(2-formylthien-5-yl)-(*E*)-ethene [14,37], and $[RuCl(dppe)_2]PF_6$ [38] were prepared following literature procedures. All reactions described below were carried out under Schlenk conditions. Tetrahydrofuran was dried by distilling over sodium/benzophenone, and dichloromethane was dried and distilled over calcium hydride. Petrol refers to a fraction of petroleum spirits with a boiling range 60-80 °C. All other reagents and solvents were sourced commercially and used as received. Chromatography was on silica gel (200-300 mesh) or basic alumina.

4.2 Instrumentation. NMR spectra were recorded using a Varian MR-400, Bruker AVANCE III-400, or Bruker ARX600 FT-NMR spectrometers, and are referenced to tetramethylsilane (^{1}H and ^{13}C, 0.00 ppm),

residual chloroform (^{1}H, 7.26 ppm; ^{13}C, 77.16 ppm), or external 85% H_3PO_4 (^{31}P, 0.00 ppm). ATR IR vibrational spectra were recorded using a PerkinElmer Spectrum Two FT-IR spectrometer as films and are reported in cm^{-1}. UV-Vis-NIR spectra were recorded as CH_2Cl_2 solutions in 1 cm quartz cells using a PerkinElmer Lambda 950 or a PerkinElmer Lambda TU1901 spectrophotometer, and are reported as λ_{max} nm (ε 10^4 mol^{-1} dm^3 cm^{-1}). Mass spectra were recorded at the Research School of Chemistry, Australian National University, using a Micromass/Water's LCT-ZMD single quadrupole liquid chromatograph-MS (ESI MS, both unit resolution and HR). Elemental analyses were carried out at the School of Human Sciences, Science Centre, London Metropolitan University, U.K. Cyclic voltammetry measurements were recorded using an e-corder 401 potentiostat from eDaq Pty Ltd; measurements were carried out at room temperature (298K) and a scan rate of 100 mV s^{-1} using Pt disc working-, Pt wire auxiliary-, and Ag/AgCl reference electrodes, such that the ferrocene/ferrocenium redox couple was located at 0.56 V (ΔE_p ca. 0.09 V**,** i_{pc}/i_{pa} = **1**). Electrochemical solutions contained 0.1 M [^{n}Bu$_4$N]PF_6 and ca. 10^{-3} M complex in dried and distilled CH_2Cl_2. Solutions were purged and maintained under a nitrogen atmosphere. Solution spectra of the oxidized species were obtained at RT by electrogeneration using a μAutolabIII potentiostat in an optically-transparent thin-layer electrochemical (OTTLE) cell constructed using a 0.5 mm path-length optical cuvette with platinum gauze working-, platinum wire counter- and silver wire reference electrodes. Solutions were made up in 0.1 M (NBu^n_4)PF_6 in deoxygenated and dry dichloromethane. The oxidation potential was set ca. 0.1 V beyond $E_{1/2}$, measured using cyclic voltammetry, to ensure complete oxidation. The reversibility was tested by applying a reducing potential to the oxidized species. A Tsunami-pumped OPAL (model Spectra-Physics) was used for HRS studies at 1300 nm. With a high repetition rate of the laser, high frequency demodulation of fluorescence contributions can be effected, a full description being given in ref. 39. All measurements were performed in THF using the internal reference method and the β value of the solvent as a reference ($\beta_{zzz,1300}$ = 0.331 x 10^{-30} esu). Experiments utilized low chromophore concentrations. The data obtained from solutions of **Ru2T** and **Ru3T** were corrected for self-absorption. The linearity of the HRS signal as a function of the chromophore concentration confirmed that no significant self-absorption of the SHG signal of **Ru1T** had occurred and so no self-absorption correction was necessary.

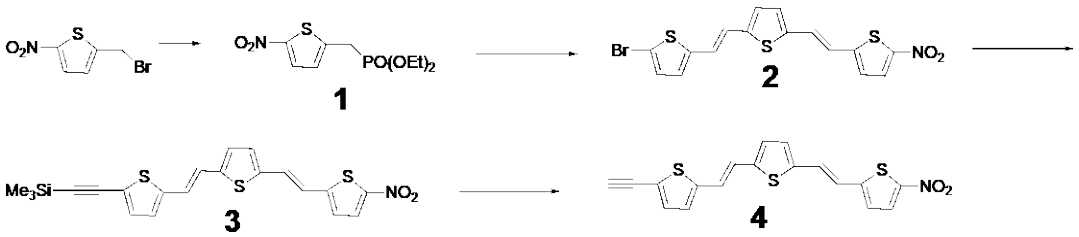

*4.3 Synthesis of diethyl ((5-nitrothiophen-2-yl)methyl)phosphonate (**1**).* A mixture of 5-(bromomethyl)-2-nitrothiophene (8.00 g, 36.0 mmol) and triethylphosphite (8.98 g, 54.0 mmol) was heated at 140°C for 5

h. The excess triethylphosphite was removed under reduced pressure. The residue was purified by column chromatography (silica gel, 1:1 CH_2Cl_2/petrol eluent) and the solvent reduced in volume, affording **1** as a light-yellow oil (9.58 g, 34.31 mmol, 95%). R_f = 0.4 (silica gel, CH_2Cl_2). ^{1}H NMR (600 MHz, $CDCl_3$): δ = 7.80 (d, J_{HH} = 6 Hz, 1H, thienyl), 6.96 (m, 1H, thienyl), 4.16 – 4.11 (m, 4H, CH_2), 3.36 (d, J_{HH} = 18 Hz, 2H, CH_2), 1.32 (t, J_{HH} = 9 Hz, 6H, Me); ^{13}C NMR (151 MHz, $CDCl_3$): δ = 142.0, 141.9, 128.7, 127.3, 63.0, 29.1 (d, J_{CP} = 140 Hz), 16.4 (d, J_{CP} = 6 Hz) ppm; ^{31}P NMR (243 MHz, $CDCl_3$) δ = 21.7 ppm; UV-Vis (CH_2Cl_2): λ_{max} (ε) = 327 (0.95); HRMS (ESI): $[M + H]^+$ *m/z* calcd for $C_9H_{15}NO_5PS$: 280.0403, found 280.0408.

*4.4 Synthesis of 2-bromo-5-((E)-2-(5-((E)-2-(5-nitrothiophen-2-yl)ethenyl)thiophen-2-yl)ethenyl)thiophene (**2**).* 1-(2-Bromothien-5-yl)-2-(2-formylthien-5-yl)-(*E*)-ethene (1.00 g, 3.34 mmol), diethyl ((5-nitrothiophen-2-yl)methyl)phosphonate (**1**; 1.40 g, 5.00 mmol), and LiCl (425 mg, 10.0 mmol) were dissolved in THF (100 mL) and the resultant solution was cooled to 0 °C. t-BuOK (1.13 g, 10.0 mmol) was added portionwise over 5 min, and the reaction was allowed to come to room temperature overnight, with stirring. The solvent was removed and the residue was washed with water (3 × 50 mL), extracted with CH_2Cl_2 (3 × 50 mL), and the combined CH_2Cl_2 extracts were dried over anhydrous Na_2SO_4 and the solvent removed. The residue was purified by column chromatography (silica gel, 5:1 petrol:CH_2Cl_2) and the solvent reduced in volume, affording **2** as a red solid (1.15 g, 2.71 mmol, 81%). R_f = 0.4 (silica gel, 2:1 petrol:CH_2Cl_2); ^{1}H NMR (400 MHz, $CDCl_3$): δ = 7.83 (d, J_{HH} = 4 Hz, 1H, thienyl), 7.20 (d, J_{HH} = 12 Hz, 1H, CH=CH), 7.06 (d, J_{HH} = 4 Hz, 1H, thienyl), 6.98 – 6.95 (m, 3H, CH=CH), 6.93 (s, 1H, thienyl), 6.89 (s, 1H, thienyl), 6.86 (s, 1H, thienyl), 6.81 (d, J_{HH} = 4 Hz, 1H, thienyl); ^{13}C NMR (151 MHz, $CDCl_3$): δ = 149.0, 148.0, 142.6, 142.5, 138.8, 129.7, 129.0, 128.7, 126.6, 125.9, 125.4, 123.6, 121.2, 120.3, 118.5, 111.0; UV-Vis (CH_2Cl_2): λ_{max} (ε) = 478 (3.4), 375 (1.5), 287 (1.1); elemental analysis calcd (%) for $C_{16}H_{10}BrNO_2S_3$: C 45.29, H 2.38, N 3.30; found: C 45.35, H 2.31, N 3.39.

*4.5 Synthesis of trimethyl((5-((E)-2-(5-((E)-2-(5-nitrothiophen-2-yl)ethenyl)thiophen-2-yl)ethenyl)thiophen-2-yl)ethynyl)silane (**3**).* $PdCl_2(PPh_3)_2$ (83 mg, 0.12 mmol), CuI (22 mg, 0.12 mmol) and HC≡CSiMe$_3$ (23 mg, 2.36 mmol) were added to a solution of **2** (500 mg, 1.18 mmol) in NEt_3 (40 mL) and CH_2Cl_2 (10 mL). The reaction mixture was heated at 70 °C under a nitrogen atmosphere for 6 h. After cooling to room temperature, the mixture was taken to dryness and the residue purified by column chromatography (silica gel, 5:1 petrol:CH_2Cl_2). The solvent was reduced in volume, affording **3** as a red solid (430 mg, 0.97 mmol, 83%). R_f = 0.4 (silica gel, 2:1 petrol:CH_2Cl_2); ^{1}H NMR (400 MHz, $CDCl_3$): δ = 7.83 (d, J_{HH} = 4 Hz, 1H, thienyl), 7.20 (d, J_{HH} = 8 Hz, 1H, thienyl/CH=CH), 7.12 (d, J_{HH} = 4 Hz, 1H, thienyl), 7.06 (d, J_{HH} = 4 Hz, 1H, thienyl), 6.99 – 6.95 (m, 4H, thienyl/CH=CH), 6.91 (d, J_{HH} = 4 Hz, 1H, thienyl), 6.88 (d, J_{HH} = 12 Hz, 1H, CH=CH), 0.26 (s, 9H, Me); ^{13}C NMR (101 MHz, DMSO-d_6) δ = 150.4,

149.4, 144.0, 143.8, 140.3, 133.9, 130.4, 130.1, 128.2, 127.0, 126.8, 125.0, 122.9, 122.2, 120.0, 101.2, 98.0, 0.2; UV-Vis (CH_2Cl_2): λ_{max} (ε) = 485 (3.8), 389 (1.6), 299 (0.95); HRMS (ESI): $[M]^+$ *m/z* calcd for $C_{21}H_{19}NO_2S_3Si$: 441.03417, found 441.03366; elemental analysis calcd (%) for $C_{21}H_{19}NO_2S_3Si$: C 57.11, H 4.34, N 3.17; found: C 57.37, H 4.11, N 3.23.

*4.6 Synthesis of 2-ethynyl-5-((E)-2-(5-((E)-2-(5-nitrothiophen-2-yl)ethenyl)thiophen-2-yl)ethenyl)thiophene (**4**).* K_2CO_3 (313 mg, 2.26 mmol) was added to a solution of **3** (500 mg, 1.13 mmol) in MeOH (100 mL) and the mixture was stirred at room temperature for 5 h, over which time a red precipitate appeared. The solid was collected and dissolved in CH_2Cl_2, dried over Na_2SO_4, filtered, the solvent removed from the filtrate, and the crude product purified by column chromatography (silica gel, 5:1 petrol:CH_2Cl_2). The solvent was reduced in volume, affording **15** as a red solid (350 mg, 0.95 mmol, 84%). R_f = 0.3 (silica gel, 2:1 petrol:CH_2Cl_2); ^{1}H NMR (600 MHz, *d*$_6$-DMSO): δ = 8.09 (d, J_{HH} = 6 Hz, 1H, thienyl), 7.61 (d, J_{HH} = 18 Hz, 1H, CH=CH), 7.37 (d, J_{HH} = 6 Hz, 1H, thienyl), 7.32 (d, J_{HH} = 3 Hz, 1H, thienyl), 7.32 (d, J_{HH} = 3 Hz, 1H, thienyl), 7.25 (d, J_{HH} = 6 Hz, 1H, thienyl), 7.24 – 7.19 (m, 3H, thienyl/CH=CH), 7.17 (m, 1H, thienyl/CH=CH), 4.71 (s, 1H, C≡CH);^{13}C NMR (101 MHz, DMSO-*d*$_6$) δ = 150.3, 143.3, 142.9, 140.2, 134.2, 131.14, 131.11, 130.7, 128.8, 127.4, 126.9, 126.0, 122.3, 121.6, 120.2, 119.7, 86.4, 76.9; UV-Vis (CH_2Cl_2): λ_{max} (ε) = 481 (4.0), 385 (1.6), 296 (1.0); HRMS (ESI): $[M]^+$ *m/z* calcd for $C_{18}H_{11}NO_2S_3$: 368.99464, found 368.99426; elemental analysis calcd (%) for $C_{18}H_{11}NO_2S_3$: C 58.52, H 3.00, N 3.79; found: C 58.28, H 3.38, N 3.32.

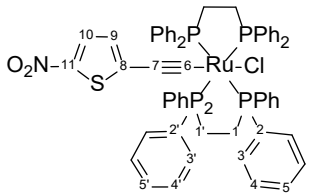

*4.7 Synthesis of **Ru1T**.* 5-Ethynyl-2-nitro-thiophene (25 mg, 0.16 mmol) and $[RuCl(dppe)_2]PF_6$ (193 mg, 0.18 mmol) were dissolved in dichloromethane (25 mL) and the solution was stirred at room temperature for 10 h, after which time NEt_3 (0.5 mL) was added, causing a colour change to purple. The solvent volume was reduced to 2 mL under vacuum and methanol (100 mL) was added, resulting in precipitation of the purple product **Ru1T**, which was washed with MeOH (3 × 10 mL) and dried in air (143 mg, 0.13 mmol, 81%). ^{1}H NMR (600 MHz, $CDCl_3$) δ = 7.72 (d, *J* = 4.4 Hz, $1H_{10}$), 7.43 (dt, *J* = 7.5, 3.4 Hz, $8H_3$), 7.23 (m, $16H_{3,5,5'}$), 7.05 (t, *J* = 7.5 Hz, $8H_{4or4'}$), 7.01 (t, *J* = 7.5 Hz, $8H_{4or4'}$), 5.76 (d, *J* = 4.4 Hz, $1H_9$), 2.72 (m, $4H_{1or1'}$), 2.63 (m, $4H_{1or1'}$); ^{13}C NMR (151 MHz, $CDCl_3$) δ = 163.3 (p, *J* = 15 Hz), 141.9, 140.2, 135.2 (m), 134.6, 133.8, 130.9, 129.42, 129.40, 127.7, 127.4, 125.4, 30.6 (p, *J* = 12 Hz). ^{31}P NMR (162 MHz, $CDCl_3$) δ = 48.0; IR (ATR): 2022 ν(RuC≡C) cm^{-1}; UV-Vis (CH_2Cl_2): λ_{max} (ε) = 541 (26.0); MS (ESI):

calc for $C_{58}H_{50}NO_2P_4SRu$ – Cl: 1050.1602 found: 1050.1556; elemental analysis calcd (%) for $C_{58}H_{50}ClNO_2P_4RuS$: C 64.18; H 4.64; N 1.29; found C 64.04; H 4.48; N 1.33 %.

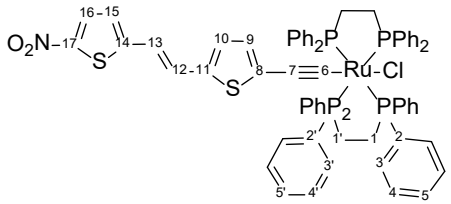

*4.8 Synthesis of **Ru2T**.* 1-(2-Nitrothien-5-yl)-2-(5-ethynylthien-2-yl)-(*E*)-ethene (30 mg, 0.11 mmol) and $[RuCl(dppe)_2]PF_6$ (148 mg, 0.14 mmol) were dissolved in dichloromethane (25 mL) and the solution was stirred at room temperature for 10 h, after which time NEt_3 (0.5 mL) was added, causing a colour change to purple. The solvent volume was reduced to 2 ml under vacuum and methanol (100 mL) was added, resulting in precipitation of the purple product **Ru2T**, which was washed with MeOH (3 × 10 mL) and dried in air (110 mg, 0.092 mmol, 80%). ^{1}H NMR (600 MHz, $CDCl_3$) δ = 7.82 (d, *J* = 4.3 Hz, 1H$_{16}$), 7.40 – 7.36 (m, 8H$_3$), 7.36 – 7.32 (m, 8H$_{3'}$), 7.22 (m, 8H$_{5,5'}$), 7.17 (d, *J* = 15.5 Hz, 1H$_{13}$), 7.02 (m, 16H$_{4,4'}$), 6.93 (d, *J* = 3.8 Hz, 1H$_{10}$), 6.90 (d, *J* = 4.3 Hz, 1H$_{15}$), 6.68 (d, *J* = 15.5 Hz, 1H$_{12}$), 6.02 (d, *J* = 3.8 Hz, 1H$_9$), 2.73 (m, 4H$_{1or1'}$), 2.69 – 2.61 (m, 4H$_{1or1'}$); ^{13}C NMR (151 MHz, $CDCl_3$) δ = 152.2, 147.6, 146.1 (p, *J* = 15 Hz), 136.1 (p, *J* = 11 Hz), 135.3 (p, *J* = 10 Hz), 134.7 – 134.5 (m), 134.2, 134.1 (d, *J* = 3 Hz), 130.7, 130.2, 129.2, 129.1, 127.9, 127.5, 127.2 (d, *J* = 3 Hz), 126.5, 123.3, 115.7, 109.0, 30.8 (p, *J* = 12 Hz); ^{31}P NMR (162 MHz, $CDCl_3$) δ = 48.8; IR (ATR): 2034 ν(RuC≡C) cm^{-1}; UV-Vis (CH_2Cl_2): λ_{max} (ε) = 400 (14.0), 604 (2.7); MS (ESI): calc for $C_{64}H_{54}NO_2P_4S_2Ru$ – Cl: 1158.1630 found: 1158.1590; elemental analysis calcd (%) for $C_{64}H_{54}ClNO_2P_4RuS_2$ C 64.40; H 4.56; N 1.17 found C 64.06; H 4.54; N 1.08 %.

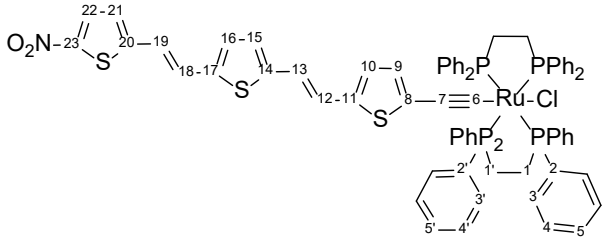

*4.9 Synthesis of **Ru3T**.* **4** (40 mg, 0.11 mmol) and $[RuCl(dppe)_2]PF_6$ (140 mg, 0.13 mmol) were dissolved in dichloromethane (25 mL) and the solution was stirred at room temperature for 10 h, after which time NEt_3 (0.5 mL) was added, causing a colour change to purple. The solvent volume was reduced to 2 mL under vacuum and methanol (100 mL) was added, resulting in precipitation of the purple product **Ru3T**, which was washed with MeOH (3 × 10 mL) and dried in air (109 mg, 0.084 mmol, 77%). ^{1}H NMR (600 MHz, $CDCl_3$) δ = 7.83 (d, *J* = 4.2 Hz, 1H$_{22}$), 7.41 (m, 8H$_3$), 7.36 (m, 8H$_{3'}$), 7.05 – 7.01 (m, 9H$_{5,5',19}$), 7.05 – 6.96 (m, 19H$_{4,4',16}$), 6.99 (d, J = 15.6 Hz, 1H$_{13}$), 6.91 (d, *J* = 4.6 Hz, 1H$_{15}$), 6.93 (d, *J* = 4.2 Hz, 1H$_{21}$), 6.84 (d, *J* = 15.7 Hz, 1H$_{18}$), 6.82 (d, *J* = 3.7 Hz, 1H$_{10}$), 6.78 (d, *J* = 15.6 Hz, 1H$_{12}$), 6.03 (d, *J* = 3.7 Hz, 1H$_9$), 3.01 – 2.31 (m, 8H$_{1,1'}$); ^{13}C NMR (151 MHz, $CDCl_3$) δ = 150.6, 148.6, 145.6, 141.1 (p, *J* = 15 Hz),

138.3, 136.1 (p, J = 10 Hz), 135.3 (q, J = 10 Hz), 134.5 (d, J = 3 Hz), 134.0 (d, J = 3 Hz), 132.1, 130.5, 129.8, 129.0, 128.9, 127.4 (t, J = 2 Hz), 127.0 (t, J = 2 Hz), 126.8, 126.0, 125.9, 124.3, 124.2, 118.6, 117.5, 108.0, 30.7 (p, J = 12 Hz); ^{31}P NMR (162 MHz, $CDCl_3$) δ = 48.9; IR (ATR): 2038 ν(RuC≡C) cm^{-1}; UV-Vis (CH_2Cl_2): λ_{max} (ε) = 454 (3.1), 586 (3.2); MS (ESI) calc for $C_{70}H_{58}NO_2P_4S_3Ru$ – Cl: 1266.1624 found: 1266.1652; elemental analysis calcd (%) for $C_{70}H_{58}ClNO_2P_4RuS_3$ C 64.58; H 4.49; N 1.08 found C 64.35; H 4.58; N 1.17 %.

Acknowledgments

We thank the Australian Research Council (ARC: DP170100408), the National Natural Science Foundation of China (51432006), the Chinese Government Ministry of Education, and the Chinese Government State Administration of Foreign Experts Affairs (111 Project: B13025). J. D. thanks the China Scholarship Council and the Australian National University for a CSC-ANU PhD Scholarship.

Supplementary data

Crystallographic studies of **Ru1T** and **Ru2T.2CH$_2$Cl$_2$**, cyclic voltammetric and UV-vis-NIR spectroelectrochemical studies of the new complexes, and theoretical studies of **Ru1T`-Ru*6*T`** are reported in the Supporting data. CCDC 1971705 (**Ru1T**) and 1971702 (**Ru2T**) contain the supplementary crystallographic data for this paper. The data can be obtained free of charge from The Cambridge Crystallographic Data Centre via www.ccdc.cam.ac.uk/structures.

References

[1] J. J. Apperloo, J.-M. Raimundo, P. Frere, J. Roncali, R. A. J. Jansen, Chem. Eur. J. 6 (2000) 1698-1707.

[2] S. Tanaka, Y. Fukui, N. Nakagawa, K. Murakami, T. N. Murakami, N. Koumura, A. Mori, Org. Lett. 18 (2016) 650-653.

[3] J. Kulhanek, F. Bures, J. Oprsal, W. Kuznik, T. Mikysek, A. Ruzicka, Asian J. Org. Chem. 2 (2013) 422-431.

[4] G. R. Whittell, I. Manners, Adv. Mater. 19 (2007) 3439-3468.

[5] B. J. Coe, in Comprehensive Coordination Chemistry II, Vol. 9, (Eds.: J. A. McCleverty, T. J. Meyer), Elsevier, Oxford, 2004, pp. 621-687.

[6] M. E. Thompson, P. E. Djurovich, S. Barlow, S. Marder, in Comprehensive Organometallic Chemistry III, Vol. 12, (Eds.: R. H. Crabtree, D. M. P. Mingos), Elsevier, Oxford, 2007, pp. 101-194.

[7] G. Grelaud, M. P. Cifuentes, F. Paul, M. G. Humphrey, J. Organomet. Chem. 751 (2014) 181-200.

[8] J. P. L. Morrall, M. P. Cifuentes, M. G. Humphrey, R. Kellens, E. Robijns, I. Asselberghs, K. Clays, A. Persoons, M. Samoc, A. C. Willis, Inorg. Chim. Acta 359 (2006) 998-1005.

[9] K. A. Green, T. C. Corkery, P. V. Simpson, M. P. Cifuentes, M. Samoc, M. G. Humphrey, Macromol. Rapid Commun. 33 (2012) 573-578.

[10] P. V. Simpson, L. A. Watson, A. Barlow, G. Wang, M. P. Cifuentes, M. G. Humphrey, Angew. Chem. Int. Ed. 55 (2016) 2387-2391.

[11] B. Gao, L. Mazur, M. Morshedi, A. Barlow, H. Wang, C. Quintana, C. Zhang, M. Samoc, M. P. Cifuentes, M. G. Humphrey, Chem. Commun. 52 (2016) 8301-8304.

[12] T. Schwich, A. Barlow, M. P. Cifuentes, J. Szeremeta, M. Samoc, M. G. Humphrey, Chem. Eur. J. 23 (2017) 8395-8399.

[13] I.-Y. Wu, J. T. Lin, J. Luo, C.-S. Li, C. Tsai, Y. S. Wen, C.-C. Hsu, F.-F. Yeh, S. Liou, Organometallics 17 (1998) 2188-2198.

[14] J.-L. Fillaut, J. Perruchon, P. Blanchard, J. Roncali, S. Golhen, M. Allain, A. Migalsaka-Zalas, I. V. Kityk, B. Sahraoui, Organometallics 24 (2005) 687-695.

[15] J.-L. Fillaut, Displ. Imag. 2 (2016) 115–134.

[16] Note that 2-nitrothienyl-5-alkynyl complexes have been reported, although no OTV examples were prepared: (a) A. Xia, J. P. Selegue, Inorg. Chim. Acta 334 (2002) 219-224. (b) T. J. L. Silva, P. J. Mendes, A. M. Santos, M. H. Garcia, M. P. Robalo, J. P. P. Ramalho, A. J. P. Carvalho, M. Büchert, C. Wittenburg, J. Heck, Organometallics 33 (2014) 4655−4671.

[17] For selected early organometallic examples, see refs: (a) J. C. Calabrese, L.-T. Cheng, J. C. Green, S. R. Marder, W. Tam, J. Am. Chem. Soc. 113 (1991) 7227-7232. (b) Z. Yuan, N. J. Taylor, Y. Sun, T. B. Marder, J. Organomet. Chem. 449 (1993) 27-37. (c) A. M. McDonagh, I. R. Whittall, M. G. Humphrey, B. W. Skelton, A. H. White, J. Organomet. Chem. 519 (1996) 229-235. (d) U. Behrens, H. Brussaard, U. Hagenau, J. Heck, E. Hendrickx, J. Kornich, J. G. M. van der Linden, A. Persoons, A. L. Spek, N. Veldman, B. Voss, H. Wong, Chem. Eur. J. 2 (1996) 98-103.

[18] M. P. Cifuentes, C. E. Powell, J. P. Morrall, A. M. McDonagh, N. T. Lucas, M. G. Humphrey, M. Samoc, S. Houbrechts, I. Asselberghs, K. Clays, A. Persoons, T. Isoshima, J. Am. Chem. Soc. 128 (2006) 10819-10832.

[19] T. Schwich, M. P. Cifuentes, P. A. Gugger, M. Samoc, M. G. Humphrey, Adv. Mater. 23 (2011) 1433-1435.

[20] N. Gauthier, N. Tchouar, F. Justaud, G. Argouarch, M. P. Cifuentes, L. Toupet, D. Touchard, J.-F. Halet, S. Rigaut, M. G. Humphrey, K. Costuas, F. Paul, Organometallics 28 (2009) 2253-2266.

[21] G. Grelaud, M. P. Cifuentes, T. Schwich, G. Argouarch, S. Petrie, R. Stranger, F. Paul, M. G. Humphrey, Eur. J. Inorg. Chem. (2012) 65-75.

[22] S. Marques-Gonzalez, D. S. Yufit, J. A. K. Howard, M. Kaupp, P. J. Low, Organometallics 33 (2014) 4947-4963.

[23] J. Du, M. S. Kodikara, G. J. Moxey, M. Morshedi, A. Barlow, C. Quintana, G. Wang, R. Stranger, C. Zhang, M. P. Cifuentes, M. G. Humphrey, Dalton Trans. 47 (2018) 4560-4571.

[24] B. A. Babgi, M. S. Kodikara, M. Morshedi, H. Wang, C. Quintana, T. Schwich, G. J. Moxey, N. Van Steerteghem, K. Clays, R. Stranger, M. P. Cifuentes, M. G. Humphrey, ChemPlusChem 83 (2018) 630-642.

[25] S. K. Hurst, M. P. Cifuentes, J. P. L. Morrall, N. T. Lucas, I. R. Whittall, M. G. Humphrey, I. Asselberghs, A. Persoons, M. Samoc, B. Luther-Davies, A. C. Willis, Organometallics 20 (2001) 4664-4675.

[26] L. Rigamonti, B. Babgi, M. P. Cifuentes, R. L. Roberts, S. Petrie, R. Stranger, S. Righetto, A. Teshome, I. Asselberghs, K. Clays, M. G. Humphrey, Inorg. Chem. 48 (2009) 3562-3572.

[27] R. H. Naulty, A. M. McDonagh, I. R. Whittall, M. P. Cifuentes, M. G. Humphrey, S. Houbrechts, J. Maes, A. Persoons, G. A. Heath, D. C. R. Hockless, J. Organomet. Chem. 563 (1998) 137-146.

[28] H. Zhang, M. Morshedi, M. S. Kodikara, G. J. Moxey, G. Wang, H. Wang, C. Quintana, R. Stranger, C. Zhang, M. P. Cifuentes, M. G. Humphrey, ChemPlusChem 81 (2016) 613-620.

[29] B. Babgi, L. Rigamonti, M. P. Cifuentes, T. C. Corkery, M. D. Randles, T. Schwich, S. Petrie, R. Stranger, A. Teshome, I. Asselberghs, K. Clays, M. Samoc, M. G. Humphrey, J. Am. Chem. Soc. 131 (2009) 10293-10307.

[30] M. P. Cifuentes, C. E. Powell, M. G. Humphrey, G. A. Heath, M. Samoc, B. Luther-Davies, J. Phys. Chem. A 105 (2001) 9625-9627.

[31] C. E. Powell, M. P. Cifuentes, J. P. L. Morrall, R. Stranger, M. G. Humphrey, M. Samoc, B. Luther-Davies, G.A. Heath, J. Am. Chem. Soc. 125 (2003) 602-610.

[32] C. E. Powell, M. G. Humphrey, M. P. Cifuentes, J. P. Morrall, M. Samoc, B. Luther-Davies, J. Phys. Chem. A 107 (2003) 11264-11266.

[33] M. P. Cifuentes, C. E. Powell, J. P. Morrall, A. M. McDonagh, N. T. Lucas, M. G. Humphrey, M. Samoc, S. Houbrechts, I. Asselberghs, K. Clays, A. Persoons, T. Isoshima, J. Am. Chem. Soc. 128 (2006) 10819-10832.

[34] T. Kinnibrugh, S. Bhattacharjee, P. Sullivan, C. Isborn, B. H. Robinson, B. E. Eichinger, J. Phys. Chem. B 110 (2006) 13512-13522.

[35] T. J. L. Silva, P. J. Mendes, A. M. Santos, M. H. Garcia, M. P. Robalo, J. P. P. Romalo, A. J. P. Carvalho, M. Büchert, C. Wittenberg, J. Heck, Organometallics 33 (2014) 4655-4671.

[36] Z. Li, X. Gao, W. Shi, X. Li, H. Ma, Chem. Commun. 49 (2013) 5859-5861.

[37] G. Manecke, M. Haertel, Chem. Ber. 106 (1973) 655-664.
[38] H. Zhao, P. V. Simpson, A. Barlow, G. Moxey, M. Morshedi, N. Roy, R. Philip, C. Zhang, M. P. Cifuentes, M. G. Humphrey, Chem. Eur. J. 21 (2015) 11843-11854.
[39] G. Olbrechts, K. Wostyn, K. Clays, A. Persoons, Opt. Lett. 24 (1999) 403-405.